Identification of Specific Sites Involved in Ligand Binding by Photoaffinity Labeling of the Receptor for the Urokinase-Type Plasminogen Activator. Residues Located at Equivalent Positions in uPAR Domains I and III Participate in the Assembly of a Composite Ligand-Binding Site†

Michael Ploug*

Finsen Laboratory, Rigshospitalet, Strandboulevarden 49, DK-2100 Copenhagen Ø, Denmark

Received May 21, 1998; Revised Manuscript Received August 10, 1998

ABSTRACT: Plasminogen activation by the urokinase-type plasminogen activator (uPA) is facilitated in the presence of cells expressing the glycolipid-anchored high-affinity receptor for uPA (denoted uPAR). Structures involved in the interaction between human uPAR and a decamer peptide antagonist of uPA binding (SLNFSQYLWS) were previously tagged by specific site-directed photoaffinity labeling [Ploug, M., Østergaard, S., Hansen, L. B. L., Holm, A., and Danø, K. (1998) *Biochemistry 37*, 3612−3622]. Replacement of the key functional residues Phe[4] and Trp[9] with either benzophenone or (trifluoromethyl)-aryldiazirine rendered this peptide antagonist photoactivatable, and as a consequence, it incorporated covalently upon photolysis into either uPAR domain I or domain III depending on the actual position of the photophore in the sequence. The residues of uPAR specifically targeted by photoaffinity labeling were identified by matrix-assisted laser desorption mass spectrometry, NH_2-terminal sequence analysis, and amino acid composition analysis after enzymatic fragmentation and HPLC purification. According to these data, the formation of the receptor−ligand complex positions Phe[4] of the peptide antagonist very close to Arg[53] and Leu[66] in uPAR domain I and Trp[9] of the antagonist in the vicinity of His[251] in uPAR domain III. The gross molecular arrangement of the deduced receptor−ligand interface provides a rational structural basis for the observed requirement for the intact multidomain state of uPAR for achieving high-affinity ligand binding, since according to this model ligand binding must rely on a close spatial proximity of uPAR domains I and III. In addition, these data suggest that the assembly of the composite ligand binding site in uPAR may resemble the homophilic interdomain dimerization of κ-bungarotoxin, a structural homologue of the Ly-6/uPAR domain family.

The cellular receptor for the urokinase-type plasminogen activator (uPAR)[1] is a glycolipid-anchored membrane glycoprotein (*1*) regulating the cell surface-associated plasminogen activation that is mediated by its natural ligand, the urokinase-type plasminogen activator (uPA). Several independent lines of experimental evidence suggest that plasminogen activation by receptor-bound uPA may play a role in the multifactorial process of tumor cell invasion and metastasis (*2*−*7*). Accordingly, clinical studies correlate poor patient prognosis with high levels of uPAR determined in extracts of tumor tissue resected from either colorectal, lung, or breast cancer patients (*8*−*10*). With a view of these important biological properties, the uPA−uPAR interaction provides an obvious and attractive molecular target for the development of low-molecular weight receptor binding antagonists that may represent potential drug candidates by interfering with cell surface-associated plasminogen activation. Affinity selections in a random 15-mer peptide library created by bacteriophage display have already identified such uPAR binding peptides, the best of which competes for uPA binding with an IC_{50} value of 10 nM (*11*). A further analysis of the molecular aspects of the specific interaction of this peptide with uPAR suggests that this antagonist and uPA may share an almost coinciding ligand-binding site on uPAR (*12*). Both ligands have several receptor binding properties in common, including the ability of the ligand to titrate the uPAR-mediated enhancement of 8-anilino-1-naphthalenesulfonate (ANS) fluorescence and the absolute requirement of an intact three-domain structure of uPAR for the maintenance of a high-affinity receptor−ligand interaction (*12*, *13*). Recently, site-directed photoaffinity labeling of the ligand interaction site on uPAR using a peptide antagonist as a photoprobe demonstrated that this receptor−ligand interface is composed of elements located in discrete structural domains of uPAR (*12*). In this study, I have been able to precisely locate those residues of uPAR affinity

† This work was supported by the Danish Cancer Society, the Danish Biotechnology Program, the NOVO-Nordic Foundation, the Astrid Thaysens Fond, and The Lundbeck Foundation.

* To whom correspondence should be addressed: Finsen Laboratory, Rigshospitalet Opg. 86.21, Strandboulevarden 49, DK-2100 Copenhagen Ø, Denmark. Telephone: +45-35455708. Fax: +45-35385450. E-mail: m-ploug@finsenlab.dk.

[1] Abbreviations: ANS, 8-anilino-1-naphthalene sulfonate; ATF, amino-terminal fragment of uPA; Bpa, *p*-benzoyl-L-phenylalanine; Fmoc, 9-fluorenylmethoxycarbonyl; GFD, epidermal growth factor-like domain of uPA; MALDI-MS, matrix-assisted laser desorption ionization mass spectrometry; (Tmd)Phe, 4′-[(trifluoromethyl)diazirinyl]-L-phenylalanine; PTH, phenylthiohydantoin; uPA, urokinase-type plasminogen activator; uPAR, uPA receptor.

10.1021/bi981203r CCC: $15.00
Published on Web 11/05/1998

labeled by these photoprobes using matrix-assisted laser desorption mass spectrometry and NH_2-terminal sequence analysis. This information provides the necessary guidelines for a future detailed study of the composite ligand binding site in uPAR by site-directed mutagenesis. In addition, a tentative gross molecular model of uPAR, including interdomain interactions, may be proposed on the basis of a comparison with other members of the Ly-6/uPAR domain family.[2]

MATERIALS AND METHODS

Chemicals and Reagents. Synthesis of *N*-(9-flourenylmethoxycarbonyl)-4′-(trifluoromethyldiazirinyl)-L-phenylalanine [Fmoc-(Tmd)Phe] was performed as described previously (*12*). Fmoc-protected *p*-benzoyl-L-phenylalanine (Bpa) was purchased from Bachem (Bubendorf, Switzerland). Bolton-Hunter reagent [*N*-succinimidyl-3-(4-hydroxy-5-[^{125}I]iodophenyl)propionate] was purchased from Amersham (Buckinghamshire, U.K). Decamer peptide antagonists containing either Bpa or Tmd(Phe) as photophores (Figure 1A) were synthesized and radiolabeled by conjugation at the NH_2 terminus as described previously (*12*).

A recombinant variant of uPAR (residues 1−277) was expressed in Chinese hamster ovary (dhfr$^-$) cells and was secreted to the medium due to a COOH-terminal truncation, which eliminates the signal sequence responsible for the glycolipid anchoring of uPAR (*1*). This recombinant soluble uPAR (for simplicity, still denoted uPAR in the following section) was purified by immunoaffinity chromatography using an anti-uPAR monoclonal antibody (*14*). Modified porcine trypsin (EC 3.4.21.4) of sequencing grade was obtained from Promega (Madison, WI). Endoproteinase Asp-N (EC 3.4.21) and recombinant *N*-glycanase (EC 3.2.2.18) from *Flavobacterium meningosepticum* expressed in *Escherichia coli* (25 units/μg) were purchased from Boehringer Mannheim.

Photoaffinity Labeling of uPAR. Photoincorporations on a preparative scale were performed in 100 μL aliquots each containing 50 μM uPAR, 100 μM photoactive peptide, and 0.2 μM corresponding ^{125}I-labeled peptide (a total of 2×10^3 cpm/μL) dissolved in 50 mM phosphate and 150 mM NaCl (pH 7.4). Photoactivation of samples was carried out for 90 min in polystyrene dishes (Nunc 96-well dishes) placed on ice with the relevant wells uniformly positioned 1−2 cm from the light source (Philips TL/09 actinic lamp, 20 W, $\lambda_{max} = 355$ nm).

Enzymatic Domain Mapping of uPAR. To liberate uPAR domain I from domains II and III by limited proteolysis, the crude photolysis mixtures containing photoaffinity-labeled uPAR conjugates were incubated for 2 h at 37 °C with porcine trypsin using an enzyme-to-substrate ratio (w/w) of 1:2000 (*15*). This method was considered favorable compared to the established chymotrypsin cleavage (*14*, *16*), since the photoactivatable peptide antagonists contain several potential cleavage sites for chymotrypsin (Trp, Tyr, and Phe), but none at all for trypsin (absence of Lys and Arg). The generated fragments were separated by size exclusion chro-

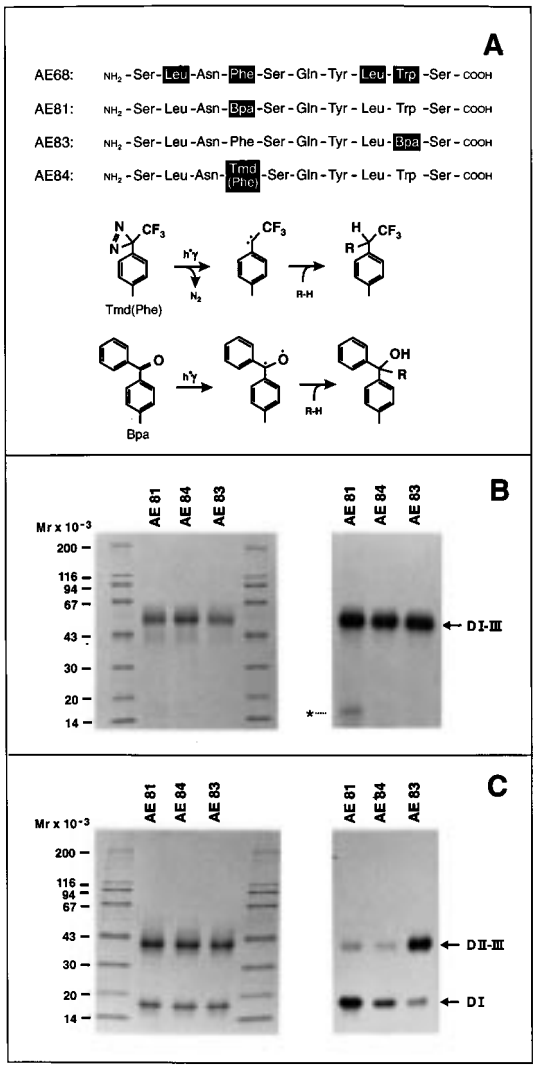

FIGURE 1: Site-specific photoaffinity labeling of uPAR. (A) The sequence of the parent decamer peptide antagonist (AE68) is shown with the residues critical for its inhibitory properties highlighted (*12*). Also shown are the sequences of the photoactivatable derivatives (AE81, AE83, and AE84) employed in the site-specific photoaffinity labeling of uPAR. The different photochemistries of the active photophores of Tmd(Phe) and Bpa are shown. Upon excitation (~350 nm), the benzophenone (Bpa) reversibly enters a n → π^* biradical triplet state, whereas the (trifluoromethyl)-aryldiazirine, Tmd(Phe), irreversibly generates a highly reactive singlet carbene by a photodissociative process. Both intermediates can enforce hydrogen abstraction on appropriately oriented target C−H bonds with a maximal range of 3.1 Å for Bpa and considerably less for Tmd(Phe). (B) Purified uPAR (20 μM) was incubated with an equimolar amount of three different ^{125}I-labeled photoactivatable derivatives of the peptide antagonist AE68, namely, AE81, AE84, and AE83. After photolysis for 45 min on ice, an aliquot of each was analyzed by SDS−PAGE (left) and then by autoradiography (right). The asterisk indicates the occurrence of a photochemical cleavage of uPAR observed only in the presence of AE81. (C) After photolabeling, samples were treated with trypsin (E:S ratio ~ 1:2000) for 2 h at 37 °C to liberate uPAR domain I (residues 1−83) from domains II and III (residues 90−277). The generated fragments were analyzed by SDS−PAGE (left) and autoradiography (right). Coomassie-stained bands corresponding to domain I and domains II and III from each labeling experiment were excised and subjected to γ-counting. The relative levels of photoinsertion into domain I were 73% for AE81 and 70% for AE84, while domains II and III incorporated 76% when AE83 was used.

[2] Recommended nomenclature as proposed by P. Bork and A. Bairoch in 1995 in *Trends in Biochemical Sciences* in volume 20 (number 3), poster C02.

matography on a Superdex HR75 column (Pharmacia LKB Biotechnology Inc., Uppsala, Sweden) using 0.1 M NH_4HCO_3 as the mobile phase.

Peptide Mapping of uPAR Domain I. Domain I isolated by size exclusion chromatography was initially deglycosylated by incubation for 6 h at 37 °C with 0.5 unit of *N*-glycanase before it was subjected to trypsin cleavage by incubation for 18 h at 37 °C with porcine trypsin at an enzyme-to-substrate ratio of 1:50 (w/w) in 0.1 M NH_4HCO_3. The generated peptides were purified by reversed-phase HPLC using a 300 Å pore size Brownlee Aquapore butyl (C4) column (2.1 mm × 100 mm) and a 60 min linear gradient from 0 to 70% (v/v) acetonitrile in 0.1% (v/v) trifluoroacetic acid at a flow rate of 300 μL/min. The elution profile was monitored at both 214 and 280 nm.

Peptide Mapping of uPAR Domains II and III. Fractions isolated with the size exclusion chromatography containing uPAR domains II and III were dried by vacuum evaporation and redissolved in 50 μL of 6 M guanidinium chloride, 25 mM EDTA, 500 mM Tris (pH 8.0), and 40 mM DTT. Complete denaturation and reduction were accomplished after incubation for 10 min at 50 °C. Subsequently, the temperature was lowered to 20 °C, and alkylation of the generated thiol groups was achieved by addition of iodoacetamide to a final concentration of 100 mM. After a 10-fold dilution in H_2O, reduced and alkylated uPAR domains II and III were deglycosylated by incubation for 2 h at 37 °C in the presence of 0.5 unit of *N*-glycanase followed by proteolysis with porcine trypsin (E:S ratio ~ 1:50 w/w) for 18 h at 37 °C. Peptide mapping by reversed-phase HPLC was performed as described above for domain I.

pH Titration of the Receptor−Ligand Interaction. The analysis of the uPA−uPAR interaction as a function of pH was performed in the following composite buffer system: 50 mM 3-(cyclohexylamino)-1-propanesulfonic acid, 50 mM Tris, 50 mM 2-[bis(2-hydroxyethyl)amino]-2-(hydroxymethyl)propane-1,3-diol, 50 mM citrate, and 0.1 M NaCl adjusted to the required pH in the range of 4.0−10.0 by titration with either HCl or NaOH. Binding kinetics of the uPA−uPAR interaction were monitored in real time by surface plasmon resonance using a Biacore2000 instrument (Pharmacia Biasensor, Uppsala, Sweden) as a function of pH. A carboxymethylated dextran matrix (CM5 sensor chip) was preactivated with *N*-hydroxysuccinimide/*N*-ethyl-*N*′-[3-(diethylamino)propyl]carbodiimide followed by coupling of uPA by injection of a 20 μg/mL solution of uPA in 10 mM sodium acetate (pH 5.0) at a flow rate of 5 μL min^{-1} for 6 min. Approximately 2000 resonance units (RU) were immobilized by this procedure. Sensorgrams (RU vs time) representing real time uPA−uPAR binding were recorded at a flow rate of 10 μL min^{-1} at 5 °C by injection of 100 nM uPAR in running buffer for 10 min. Running buffer was the previously mentioned composite buffer including 0.005% surfactant P-20 after subsequent adjustment to the relevant pH. Levels of receptor binding were measured 7.5 min after initiation of analyte injection (uPAR). Changes due to the difference in the bulk refractive index were subtracted using a parallel mock coupled flow cell.

Miscellaneous Analyses. Amino acid composition analyses were carried out using a Waters amino acid analyzer with *o*-phthaldialdehyde derivatization and HPLC anion exchange chromatography. Acid hydrolysis was achieved by incubation in vacuo at 110 °C for 20 h in 6 M HCl containing both phenol and 3,3′-dithiodipropionic acid at 0.05% (w/v) (*17*). NH_2-Terminal sequence analyses were performed on an Applied Biosystems 477A pulsed-liquid automated protein sequencer interfaced with an Applied Biosystems 120A PTH analyzer. Mass analyses were obtained by matrix-assisted laser desorption ionization (MALDI-MS) using a linear time-of-flight mass spectrometer (Voyager, PerSeptive Biosystems) equipped with a 1.2 m flight tube and a 337 nm nitrogen laser. All spectra were recorded after sample deposition in α-cyano-4-hydroxycinnamic acid (*18*) and were calibrated internally using appropriate matrix ions as a reference mass.

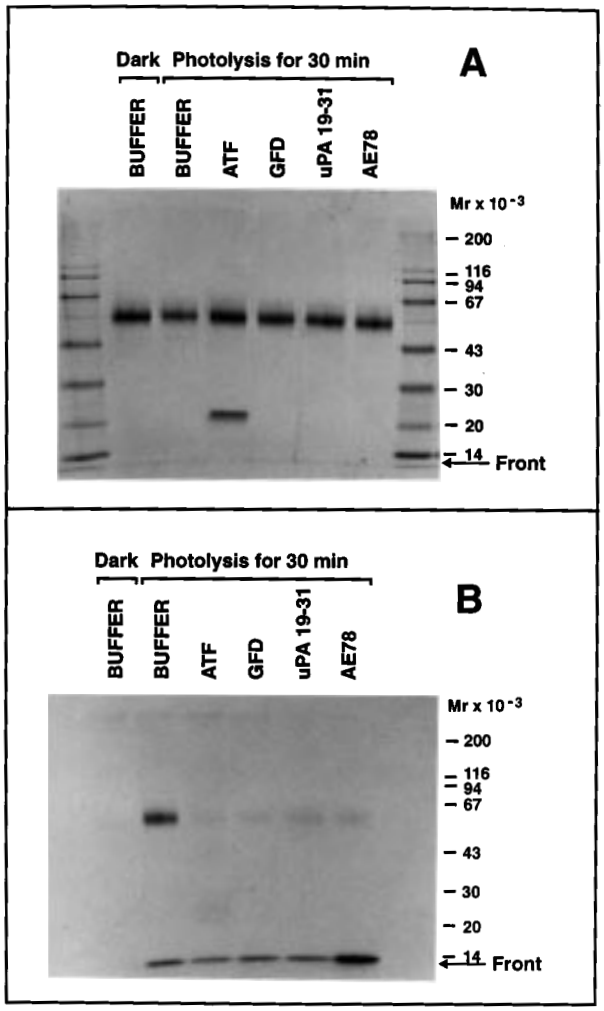

FIGURE 2: Site-specific photoaffinity labeling of uPAR is inhibited by preincubation with receptor binding derivatives of uPA. Purified uPAR (20 μM) was preincubated for 5 min with a 2-fold molar excess of ATF, GFD, uPA_{19-31}, AE78, or buffer before the addition of 20 μM ^{125}I-labeled AE84 and subsequent photolysis for 30 min. These samples were analyzed by SDS−PAGE, of which the Coomassie-stained polyacrylamide gel (A) and corresponding autoradiography (B) are shown. ATF is the amino terminal fragment of uPA (residues 6−135). GFD is the growth factor-like domain of uPA (residues 4−43). uPA_{19-31} is a synthetic, cyclic peptide derived from the ω-loop of uPA with a non-natural, terminal disulfide bond introduced (CVSNKYFSNIHWC). AE78 is a 17-mer synthetic, linear peptide antagonist originally identified by phage display technology (AEPMPHSLNFSQYLWYT).

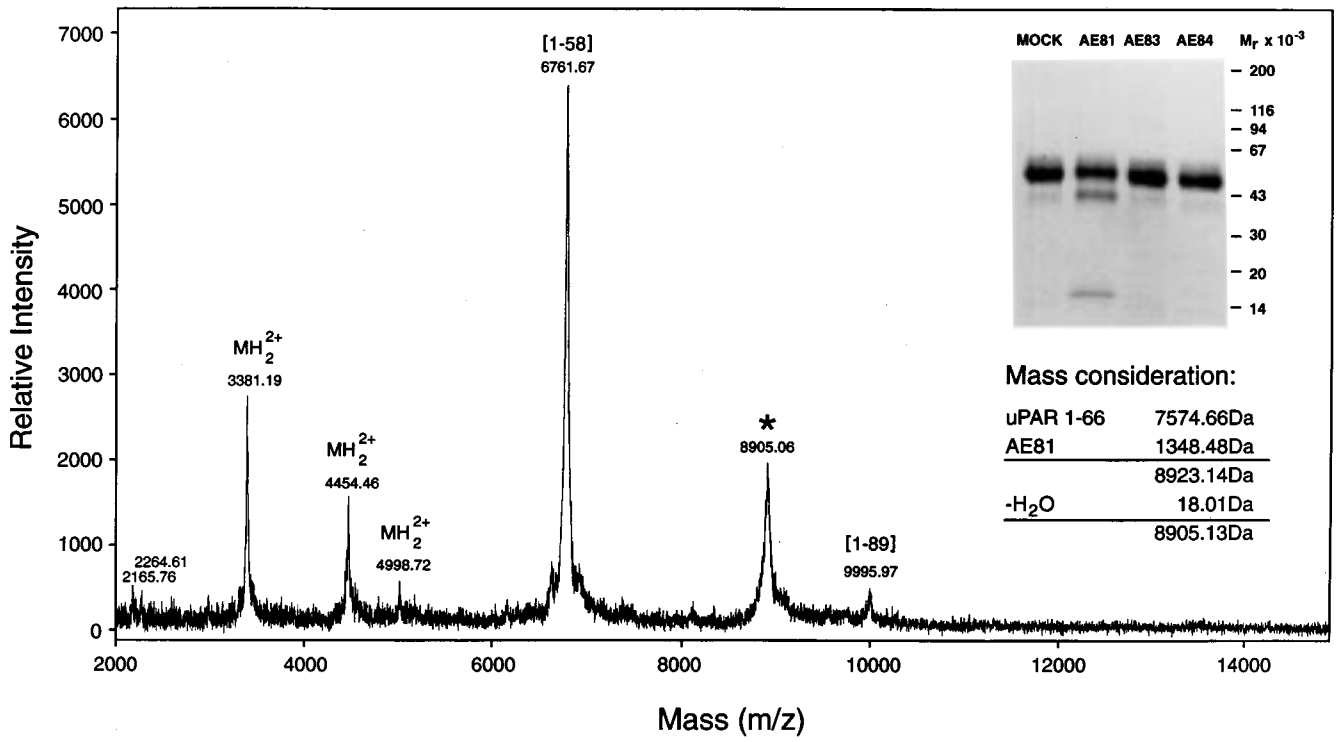

FIGURE 3: Specific photochemical fragmentation of uPAR domain I by AE81. Purified uPAR (50 μM) was subjected to preparative photolysis in the presence of buffer (mock) or 100 μM photoactivatable peptide (AE81, AE83, or AE84), including a trace amount of the corresponding ^{125}I-labeled peptide (0.2%). The inset shows a 12% polyacrylamide gel after SDS−PAGE and Coomassie staining of the photolyzed samples (unreduced). An aliquot of uPAR photolyzed in the presence of AE81 was subjected to analytical size exclusion chromatography to separate the observed photochemical fragmentation product from the remaining intact uPAR. As this product proved to contain carbohydrate, it was deglycosylated by *N*-glycanase treatment before analysis by MALDI-MS. This spectrum reveals the presence of a hitherto unknown degradation product of uPAR having a molecular mass of 8904.1 Da (marked with an asterisk) in addition to the well-established "auto-degradation" products of uPAR (*13*) generated by enzymatic cleavage after Arg^{58} (6760.7 Da) and Arg^{89} (9997.4 Da). The theoretical masses of peptides made up of residues 1−58, 1−66, and 1−89 have been corrected for the Asn → Asp transition of Asn^{52} caused by the action of the catalytic mechanism of *N*-glycanase. The mass assignments are those of the molecular ions (MH^+).

RESULTS

Analytical Photoaffinity Labeling of Intact uPAR Using Decamer Peptide Antagonists. The interaction between purified human uPAR and a 15-mer peptide antagonist selected with a bacteriophage display technique (*11*) has previously been studied in detail, including the tailoring of an active minimal decapeptide antagonist (AE68) and the identification of residues critical for its antagonistic properties (see Figure 1A and ref *12*). Replacement of either Phe^4 or Trp^9 in this peptide with the photophores, Tmd(Phe) or Bpa, led to peptide derivatives, which were incorporated covalently into uPAR upon exposure to UV light. A gross domain mapping of this specific photoinsertion using limited proteolysis with chymotrypsin revealed the presence of a composite ligand binding site in uPAR. Photoprobes replacing Phe^4 of the peptide antagonist were thus shown to be incorporated into uPAR domain I, while a photoprobe positioned at Trp^9 was incorporated into domain II or III of uPAR (*12*). The main focus of this study is to identify these targeted amino acid residues of uPAR. Therefore, we initially attempted to increase the yields of productive photoinsertion compared to those obtained previously (2−5%) by elevating 4-fold the concentrations of both uPAR and the photoactivatable peptides to final concentrations of 20 μM. This improved the yields significantly, since approximately 20% of the peptide was incorporated as determined by γ-counting (Figure 1B). As the peptide antagonist AE68 contains several potential cleavage sites for chymotrypsin, but none for trypsin, the photochemical conjugates were treated with trypsin instead of chymotrypsin to liberate domain I (Figure 1C).

These minor modifications did not impair the site specificity of the photoaffinity labeling, since it still exhibited a preferred insertion (>70% of the incorporated label) either into uPAR domain I by the photoprobes AE81 and AE84 or into uPAR domains II and III by AE83 (see Figure 1C), and this was inhibited by preincubation with a 2-fold molar excess of other receptor ligands (Figure 2). The only notable difference was the formation of an ^{125}I-labeled fragment of uPAR when photolysis was performed in the presence of 20 μM ^{125}I-labeled AE81, marked with an asterisk in Figure 1B.

Preparative Photoaffinity Labeling of uPAR with AE81, AE83, and AE84. To obtain sufficient material to localize the actual targets for the specific photoinsertion reactions at the amino acid level, preparative photoaffinity labeling experiments were performed using 50 μM uPAR and the respective photoprobes at 100 μM. Only trace quantities of ^{125}I-labeled peptides (0.2%) were included in these experiments to facilitate calculation of incorporation yields. After photolysis, aliquots representing each photoprobe were subjected to SDS−PAGE (Figure 3, inset), the Coomassie stained bands were excised, and the labeling efficiencies were estimated after γ-counting. This revealed a comparable labeling efficiency for all three photoprobes, which was compatible with the occurrence of a single photoinsertion

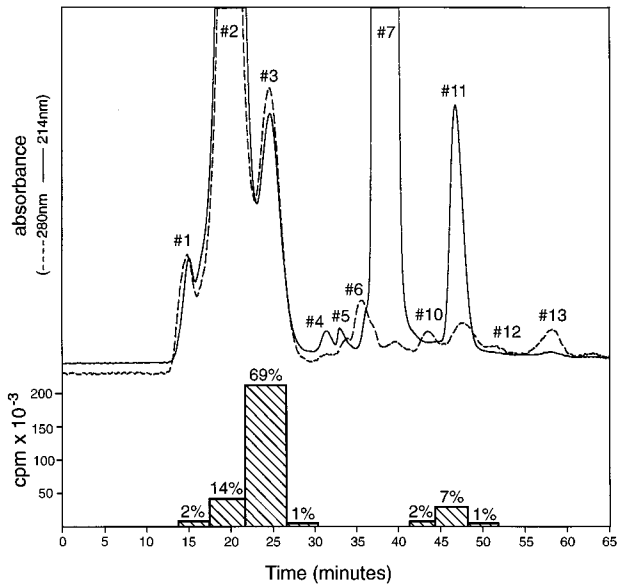

FIGURE 4: Size exclusion chromatography of trypsin-treated uPAR after photoaffinity labeling with AE81. Photochemically induced conjugates between uPAR and AE81 were subjected to limited proteolysis using trypsin to liberate domain I from domains II and III. The generated fragments were subsequently purified by size exclusion chromatography using a Superdex HR75 column and 0.1 M NH_4HCO_3 as the solvent. Elution positions of domains II and III and domain I correspond to #2 and #3, respectively. The theoretical "salt peak" of this particular size exclusion column coincides with #7. Nonincorporated AE81 only eluted during regeneration of the column with ethanol. The effluent was monitored by absorbance at 280 (- - -) and 214 nm (—) and by γ-counting of fractions manually collected (see the bottom panel).

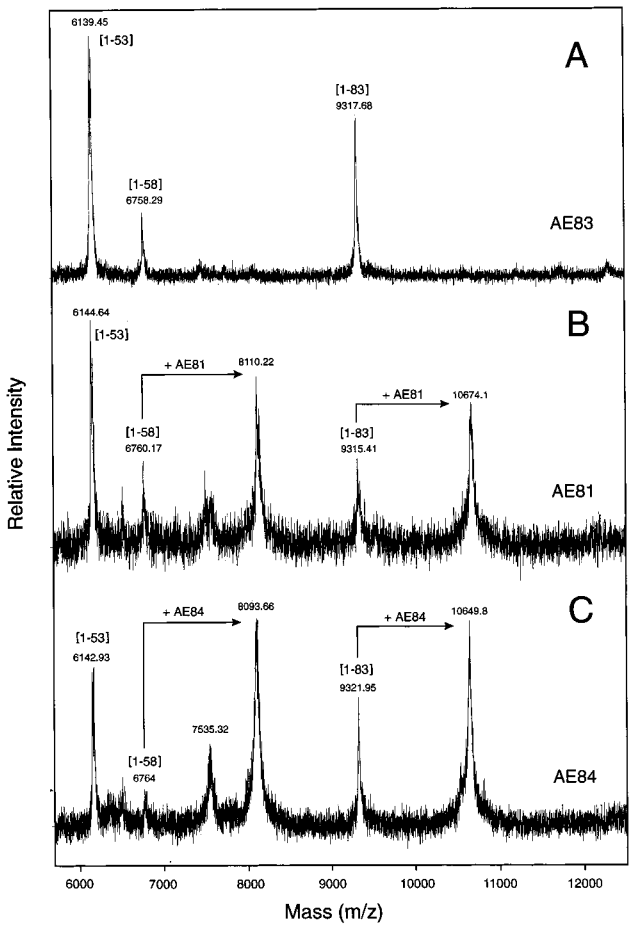

FIGURE 5: MALDI-MS spectra of photoaffinity-labeled uPAR domain I. uPAR subjected to preparative photoaffinity labeling with AE81, AE83, or AE84 was treated with trypsin to liberate domain I. This domain was subsequently purified by size exclusion chromatography (see Figure 4), a small aliquot of which was treated with *N*-glycanse to remove the carbohydrate moiety on Asn^{52} and analyzed by MALDI-MS. Panel A shows the resultant spectrum obtained for uPAR domain I after photolysis in the presence of AE83. This spectrum is comparable to the one obtained for the mock treated sample and shows no indications of photoinsertion into domain I. The photolabeling patterns of the uPAR domain I derived from photolysis of intact uPAR in the presence of AE81 and AE84 are shown in panels B and C, respectively. Productive photoinsertions are accompanied with a theoretical mass increase of 1348.4 Da for AE81 or 1324.4 Da for AE84 [corrected for the loss of N_2 during excitation of Tmd(Phe)].

into approximately 50% of the receptor molecules (data not shown).

The photochemical fragmentation of uPAR induced by the insertion of AE81 was also consistently observed during these preparative photolysis experiments (Figure 3, inset). To identify this fragment, it was therefore purified by analytical size exclusion chromatography, deglycosylated with *N*-glycanase, and finally subjected to MALDI-MS. As shown in Figure 3, the molecular mass of the unique fragment formed in the presence of AE81 was determined to be 8904.1 Da and most likely represents a covalent conjugate between $uPAR_{1-66}$ and AE81 (see mass considerations in Figure 3). This would, however, require the breakage of the peptide bond between Leu^{66} and Thr^{67}, a cleavage that is likely to preclude enzymatic hydrolysis. A possible reaction mechanism for this chemical fragmentation is presented later (Figure 6).

After preparative photolysis, the crude mixtures containing covalent conjugates between uPAR and the various peptide antagonists were treated with trypsin (E:S ratio $\sim$ 1:2000 w/w) to liberate the uPAR domain I. After purification by size exclusion chromatography (data for the experiment with AE81 are shown in Figure 4), uPAR domain I was deglycosylated to simplify the interpretation of subsequent MALDI-MS analysis (Figure 5). In accordance with data obtained previously, only AE81 and AE84 exhibit a significant level of incorporation into uPAR domain I. Furthermore, the spectra clearly demonstrate that the site-specific photoaffinity labeling of uPAR domain I with either AE81 or AE84 is univalent as there is no indication in these spectra of the occurrence of multiple peptide conjugations (Figure 5B,C).

Identification of Arg^{53} as the Primary Site in uPAR Domain I Labeled by a Benzophenone Moiety Replacing Phe^4 of the Peptide Antagonist (AE81). The size exclusion profile of uPAR photolyzed in the presence of AE81 and treated with trypsin is shown in Figure 4. In accordance with the analytical photolabeling experiments (Figure 1C), preferred labeling of uPAR domain I was observed by γ-counting (eluting in #3). A similar elution profile was obtained for labeling with AE84. In contrast, AE83 resulted in a predominant labeling of uPAR domains II and III (eluting in #2). Comparison of the three elution profiles revealed four peaks unique to the size exclusion chromatogram from labeling with AE81 (#4, #5, #11, and #12 in Figure 4). These fractions represented approximately 10% of the incorporated AE81. The vast majority of the incorporated AE81 ($\sim$70%) was however retrieved in #3 of the size exclusion chromatogram, at an elution position corresponding to uPAR

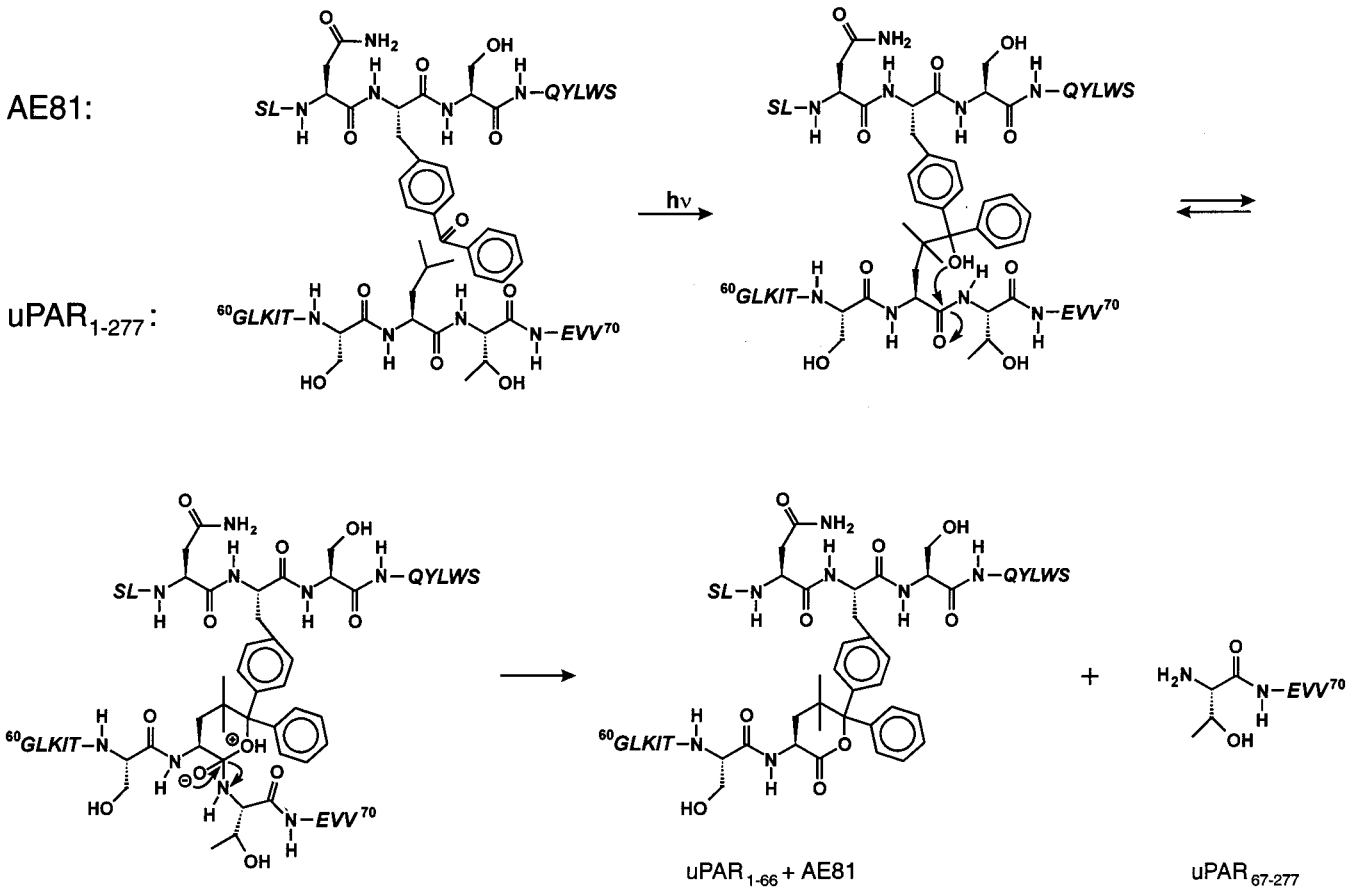

FIGURE 6: Proposed reaction mechanism for the specific chemical fragmentation at Leu[66] and Thr[67] by photoinsertion of AE81 into uPAR domain I. On photoactivation, the biradical triplet state of Bpa enforces hydrogen abstraction from the electron rich tertiary Cγ−H bond of Leu[66], one of the preferred hydrogen donors among the amino acid side chains. The tertiary alcohol of the resultant benzpinacol-type structure subsequently attacks the carbonyl group of the adjacent peptide bond. Being acid-catalyzed, this reaction would normally require a low pH as applies for the related N → O acyl shifts observed at Ser/Thr hydroxyl groups during Edman sequencing (*39*). The formation of a six-membered cyclic intermediate compared to that of the five-membered ring for N → O acyl shifts may however facilitate the proposed reaction mechanism at neutral pH. The subsequent leaving of the adjacent amino group causes the cleavage of the peptide bond between Leu[66] and Thr[67]. The observed "loss of H_2O" from the photochemical conjugates is implicit in the proposed insertion into the Cγ−H bond of Leu[66] due to the consequent formation of a stable lactone at the former COOH terminus of Leu[66].

domain I (Figure 4). The deglycosylated conjugate between uPAR domain I and AE81 (Figure 5B) was therefore subjected to an additional trypsin cleavage, and the generated polypeptides were separated by reversed-phase HPLC. Finally, the elution profile was scanned by MALDI-MS. Comparison of the determined peptide masses with those generated by a theoretical trypsin cleavage of the entire sequence of human uPAR singled out the peptide mass 2358.5 Da as the only possible candidate representing a tryptic conjugate with AE81, suggesting that this peptide represented a covalent conjugate between $uPAR_{51-58}$ and AE81 (Table 1, top section). After additional purification by reversed-phase HPLC, the peptide conjugate was subjected to both amino acid composition analysis (Table 2, column 3) and NH_2-terminal sequence analysis (Table 3, middle section). These analyses confirmed the identity of the peptide conjugate and demonstrated unambiguously that Arg[53] was the major target in uPAR for the specific insertion reaction of the activated biradical triplet state of the benzophenone moiety in AE81. The assignment of this particular cross-linking site also provides an explanation for the observed incomplete tryptic cleavage of $uPAR_{51-58}$ in the recovered conjugate.

Photoinsertion into Leu[66] by Bpa in AE81 Is Responsible for the Specific Chemical Fragmentation of the Polypeptide Chain in uPAR Domain I. As mentioned previously, size exclusion chromatography reveals several peaks unique to trypsin-treated uPAR photolyzed in the presence of AE81 (# 4, #5, #11, and #12 in Figure 4). When these fractions were analyzed by MALDI-MS, it was evident that none of the masses recorded for these peaks represented typical tryptic peptides derived from the sequence of uPAR (Table 1, middle section). As no radioactivity was associated with either #4 or #5, they were unlikely to represent photochemical conjugates with AE81. Subsequent evaluation of their molecular masses (Table 1, middle section) combined with the amino acid composition analysis determined for one of the peptides (Table 2, column 1) unambiguously disclosed their identities as $uPAR_{67-83}$ and $uPAR_{67-89}$. Since the peptide bond between Leu[66] and Thr[67] is an unlikely cleavage site for trypsin, this observation suggests a chemical fragmentation of uPAR induced by the specific insertion of AE81 into Leu[66] (Figures 3 and 6). In light of this finding and the radioactivity associated with fractions #11 and #12 (Figure 4), these were suspected to contain photochemical conjugates between AE81 and Leu[66] of uPAR, which would also account

Table 1: Summary of MALDI-MS Mass Assignments for Selected Tryptic Peptides Derived from uPAR Subjected to Site-Directed Photoaffinity Labeling in the Presence of either AE81 or AE84

Sample identity	Determined mass (MH^+)	Putative sequence identity		
		MW (Da)[a]	Residues	cDNA derived sequence[b]
AE81 #3 trypsin #4	2,359.5	2,359.59	[51-58] + AE81	EK···**TNRTLSYR**···TG **SLN-*Bpa*-SQYLWS**
AE81 #4	1,762.9	1,762.94	[67-83]	SL···**TEVVCGLDLCNQGNSGR**···AV
	2,439.9	2,440.70	[67-89]	SL···**TEVVCGLDLCNQGNSGRAVTYSR**···SR
AE81 #11	2,163.2	2,162.37	[59-66] + AE81 - H_2O	YR···**TGLKITSL*****···TE **SLN-*Bpa*-SQYLWS**
AE81 #12	1,763.5	1,762.87	[63-66] + AE81 - H_2O	LK···**ITSL*****···TE **SLN-*Bpa*-SQYLWS**
	2,782.1	2,783.03	[54-66] + AE81 - H_2O	NR···**TLSYRTGLKITSL*****···TE **SLN-*Bpa*-SQYLWS**
AE84 #3 trypsin #4	2,335.7	2,335.51	[51-58] + AE84	EK···**TNRTLSYR**···TG **SLN-*Tmd(Phe)*-SQYLWS**
AE84 #3 trypsin #3	3,498.2	3,499.82	[63-83] + AE84	LK···**ITSLTEVVCGLDLCNQGNSGR**···AV **SLN-*Tmd(Phe)*-SQYLWS**

[a] The average molecular masses of these peptides were calculated using the program GPMAW version 3.03. When two cysteine residues are present in the cDNA-derived sequence, the mass of cystine is used. If the sequence includes Asn^{52}, the mass of Asp is used due to the Asn → Asp conversion caused by the action of the catalytic mechanism of *N*-glycanse. [b] Sequences in bold represent the putative sequence identity corresponding to the determined mass of the peptide. Two residues located NH_2- and COOH-terminally with respect to the relevant sequence are shown to specify the peptide bonds that are cleaved. The asterisks denote the formation of a stable lactone involving the carbonyl groups of both Bpa and Leu^{66} (see the proposed reaction mechanism in Figure 6). The sites of photoinsertion of Bpa or Tmd(Phe) are indicated by vertical bars and were assigned by subsequent NH_2-terminal sequence analysis (Table 3) and/or amino acid composition analysis (Table 2).

for the peptide masses determined by MALDI-MS (Table 1, middle section). Two additional experiments were therefore performed to validate this interpretation. First, #11 thought to represent a covalent conjugate between AE81 and $uPAR_{59-66}$ was subjected to amino acid composition analysis after additional purification by reversed-phase HPLC. As shown in Table 2 (column 2), the derived amino acid composition confirmed the identity of the peptide conjugate and also revealed the possible involvement of a leucine residue as a target for the photochemical insertion reaction, since this was the only amino acid deviating significantly from the theoretical composition. Second, NH_2-terminal sequence analysis of a conjugate between AE81 and $uPAR_{63-66}$ yielded the expected double sequence except for an assignment lacking Leu^{66} at cycle 4 (Table 3, left section). Although it is the COOH-terminal residue, this demonstrates that Leu^{66} is the actual target for the photoinsertion of AE81 since the yields of PTH-amino acids recovered at the three preceding cycles preclude a significant conjugation at these sites.

Arg^{53} in uPAR Domain I Is Also the Primary Target for the Photoinsertion When Phe^4 of the Peptide Antagonist Is Replaced by (Trifluoromethyl)aryldiazirine (AE84). Since the Bpa moiety of AE81 represents a relatively bulky substituent for Phe^4 in the peptide antagonist, a second photoactivatable derivative was prepared (AE84), in which Phe^4 was replaced with Tmd(Phe). This highly potent carbene-generating precursor exhibits a completely different photochemistry compared to the biradical triplet generating benzophenone of AE81 (Figure 1A and ref *19*). Under identical photolysis conditions, the Tmd(Phe) photophore of AE84 caused a specific photoaffinity labeling of uPAR domain I with an efficiency comparable to that achieved by Bpa in AE81 (Figures 1 and 4) but without the subsequent photochemical fragmentation of uPAR (Figures 1 and 3). Consequently, the vast majority of the incorporated AE84 was recovered in association with uPAR domain I after limited trypsin treatment and size exclusion chromatography. Purified uPAR domain I labeled with AE84 was therefore deglycosylated with *N*-glycanase and cleaved by trypsin. The generated peptides were purified by reversed-phase HPLC and the collected fractions analyzed by MALDI-MS. Only two of the molecular masses determined qualified as suitable candidates for peptide conjugates with AE84 (Table 1, bottom section). The most abundant of these was a 2334.7 Da conjugate, possibly representing $uPAR_{51-58}$ in cross-linkage with AE84 (the theoretical mass of which is 2335.5 Da). Consistent with this, amino acid composition analysis

Table 2: Amino Acid Composition Analysis of Reversed-Phase HPLC-Purified Tryptic Peptides Derived from uPAR Subjected to Site-Directed Photoaffinity Labeling in the Presence of either AE81 or AE84[a]

sample	AE81 #4	AE81 #11	AE81 #3 (trypsin #4)	AE84 #3 (trypsin #4)	AE84 #3 (trypsin #3)
Asx	2.97 (3)	1.20 (1)	2.10 (2)	1.97 (2)	3.92 (4)
Thr[b]	1.02 (1)	1.95 (2)	1.81 (2)	1.94 (2)	1.85 (2)
Ser[b]	1.03 (1)	4.39 (4)	3.81 (4)	3.82 (4)	4.79 (5)
Glx	1.95 (2)	1.24 (1)	1.75 (1)	1.40 (1)	3.31 (3)
Pro	0.02	0.06	0.16	0.10	0.22
Gly	3.01 (3)	1.36 (1)	0.71	0.41	3.25 (3)
Ala	0.05	0.12	0.20	0.25	0.30
Cys[c]	2.09 (2)	0.00	0.39	0.46	1.99 (2)
Val	1.29[d] (2)	0.07	0.22	0.13	1.25[d] (2)
Met	0.01	0.00	0.12	0.09	0.11
Ile	0.02	0.94 (1)	0.12	0.07	0.95 (1)
Leu	2.02 (2)	**3.15 (4)**	2.86 (3)	2.91 (3)	**3.91 (5)**
Tyr	0.01	0.97 (1)	1.59 (2)	1.71 (2)	0.89 (1)
Phe	0.01	0.05	0.02	0.07	ND[e]
His	0.03	0.13	0.36	0.21	0.32
Lys	0.03	1.03 (1)	0.56	ND[e]	0.29
Arg	1.00 (1)	0.08	**1.02 (2)**	**1.03 (2)**	1.16 (1)
Trp	ND[e]	ND[e] (1)	ND[e] (1)	ND[e] (1)	ND[e]
identity	residues 67−83	residues 59−66 and AE81	residues 51−58 and AE81	residues 51−58 and AE84	residues 63−83 and AE84

[a] Values in parentheses correspond to the theoretical number for the assigned identity of the respective peptides. [b] These hydroxy amino acids are corrected for their decomposition during acid hydrolysis, Ser (10%) and Thr (5%). [c] Cysteine was determined as the mixed disulfide formed between cystine and 3,3′-dithiodipropionic acid during hydrolysis (*17*). [d] Valine is often underestimated due to incomplete release during acid hydrolysis for 20 h; this is especially pronounced for these two peptides containing a Val-Val[70] motif in their sequence (14). [e] ND means not determined. The lack of quantification was caused either by decomposition during acid hydrolysis (Trp) or by interference from the photo-cross-linked conjugate, which coeluted with that particular amino acid (Lys or Phe).

Table 3: NH_2-Terminal Amino Acid Sequence Analysis of Reversed-Phase HPLC-Purified Tryptic Peptides Representing Photochemical Conjugates between uPAR and either AE81 or AE84[a]

	AE81 #11 and #12[b]		AE81 #3 (trypsin #4)		AE84 #3 (trypsin #4)	
cycle	assignments (uPAR/AE81)	yield (pmol)	assignments (uPAR/AE81)	yield (pmol)	assignments (uPAR/AE84)	yield (pmol)
1	Ile[63]/Ser	120/66	Thr[51]/Ser	313/217	Thr[51]/Ser	322/198
2	Thr[64]/Leu	110/150	Asp[52]/Leu	328/359	Asp[52]/Leu	260/377
3	Ser[65]/Asn	55/105	**Arg[53]**/Asn	***x***/207	**Arg[53]**/Asn	***x***/226
4	**Leu[66]/Bpa**	***x***/***x***	Thr[54]/**Bpa**	164/***x***	Thr[54]/**Tmd(Phe)**	279/***x***
5	−/Ser	*x*/67	Leu[55]/ Ser	182/96	Leu[55]/ Ser	335/156
6	−/Gln	*x*/97	Ser[56]/ Gln	55/150	Ser[56]/ Gln	168/115
7	−/Tyr	*x*/50	Tyr[57]/ Tyr	192	Tyr[57]/ Tyr	320
8	−/Leu	*x*/70	Arg[58]/ Leu	61/186	Arg[58]/ Leu	147/194
9	−/Trp	*x*/36	−/Trp	*x*/46	−/Trp	*x*/90
10	−/Ser	*x*/*x*	−/Ser	*x*/*x*	−/Ser	*x*/17

[a] Experimental sequence assignments corresponding to uPAR-derived sequences are numbered according to the cDNA-derived sequence, omitting the signal sequence (*38*). Although uPAR contains an Asn residue at position 52, the present sequence analyses assigned Asp to this position due to the Asn → Asp conversion introduced by the preceding enzymatic deglycosylation by *N*-glycanse. − indicates the end of the respective uPAR-derived peptides as calculated from comparison of cDNA-derived sequences and masses measured by MALDI-MS analysis. *x* indicates no positive sequence assignment in that particular cycle. [b] #11 and #12 were combined, cleaved with trypsin, and purified by reversed-phase HPLC before sequence analysis of a peptide conjugate having a molecular mass of 1763.2 Da as determined by MALDI-MS.

(Table 2, column 4) and NH_2-terminal sequence analysis (Table 3, right section) clearly demonstrated that the Tmd-(Phe) was covalently cross-linked to Arg[53]. The less abundant peptide (3497.2 Da) possibly represents a conjugate between $uPAR_{63-83}$ and AE84 (Table 1, bottom section). Subsequent amino acid composition analysis substantiated this assignment and identified leucine as the cross-linking moiety of uPAR (Table 2, column 5). This is consistent with the labeling of Leu[66] by AE81, although this was not unambiguously demonstrated as this particular peptide also contains two other leucine residues.

Identification of His[251] as the Specific Cross-Linking Site in uPAR Domains II and III by a Benzophenone Moiety Replacing Trp[9] of the Peptide Antagonist (AE83). Photoaffinity labeling of intact uPAR with AE83 occurs primarily by a specific insertion into domains II and III (Figure 1C). This conjugate was purified by size exclusion chromatography after liberation by limited proteolysis using trypsin. Being highly glycosylated and internally cross-linked by numerous disulfide bonds, uPAR domains II and III are expected to be rather compact and resistant to proteolysis under nondenaturing conditions. The purified conjugate between AE83 and uPAR domains II and III was therefore reduced, alkylated, and deglycosylated before digestion with porcine trypsin. Subsequent peptide mapping by reversed-phase HPLC and MALDI-MS revealed only one peptide (4579.0 Da) that could not be recognized as a tryptic peptide derived from the sequence of human uPAR. This mass was however compatible with a covalent conjugate between AE83 and $uPAR_{240-268}$, part of domain III (Table 4), although the purity of this preparation was not sufficiently high to justify a direct sequencing attempt. Fortuitously, the putative

Table 4: Summary of MALDI-MS Mass Assignments for Selected Tryptic Peptides Derived from uPAR Subjected to Site-Directed Photoaffinity Labeling in the Presence of AE83

Sample identity	Determined mass (MH^+)	Putative sequence identity		
		MW (Da)[a]	Residues	cDNA derived sequence[b]
AE83 #2 trypsin #14	4,580.0	4,577.14	[240-268] + AE84	VR···**GCATASMCQHAHLGDAFSMNHIDVSCCTK**···SG **SLNFSQYL-*Bpa*-*S***
AE83 #2 trypsin #14 Asp-N #15	2,811.1	2,810.14	[240-253] + AE84	VR···**GCATASMCQHAHLG**···DA **SLNFSQYL-*Bpa*-*S***

[a] The average molecular masses of these peptides were calculated using the program GPMAW version 3.03. When cysteine is present, the mass of *S*-(carboxamidomethyl)cysteine was used. [b] Bold sequences represent the assumed sequence identity corresponding to the determined mass of the peptide. Two residues located NH_2- and COOH-terminally with respect to the sequence in question are shown to distinguish the peptide bonds cleaved. The sites of photoinsertion from Bpa are indicated by vertical bars and were assigned by a subsequent NH_2-terminal sequence analysis (Table 5).

Table 5: NH_2-Terminal Amino Acid Sequence Analysis of the Reversed-Phase HPLC-Purified Photochemical Conjugate between uPAR and AE83[a]

	AE83 #2 (trypsin #14/Asp-N #15)	
cycle	assignments (uPAR/AE83)	yield (pmol)
1	Gly^{240}/Ser	204/208
2	Cys^{241}/Leu	111/206
3	Ala^{242}/Asn	135/127
4	Thr^{243}/Phe	112/224
5	Ala^{244}/Ser	138/88
6	Ser^{245}/Gln	52/175
7	Met^{246}/Tyr	124/137
8	Cys^{247}/Leu	52/162
9	Gln^{248}/**Bpa**	73/***x***
10	His^{249}/Ser	28/(4)
11	Ala^{250}/−	57/*x*
12	**His^{251}**/−	***x***/*x*
13	Leu^{252}/−	34/*x*
14	Gly^{253}/−	(3)/*x*

[a] During sequencing, cysteines were assigned to cycles number 2 and 8 due to the identification of the PTH derivative of *S*-(carboxamidomethyl)cysteine. − indicates the end of the peptide antagonist. *x* indicates no positive sequence assignment in that particular cyclus.

uPAR-derived polypeptide sequence (29-mer) of the conjugate contained two Asp residues, not present in AE83. The isolated conjugate was therefore subjected to an additional proteolytic cleavage using the endoproteinase Asp-N and the resultant peptides purified by reversed-phase HPLC and characterized by MALDI-MS. This approach yielded a pure peptide conjugate with a molecular mass of 2810.1 Da likely to represent AE83 cross-linked to $uPAR_{240-253}$ (theoretical mass of 2810.4 Da). Subsequent NH_2-terminal sequence analysis confirmed this identity and demonstrated unambiguously that His^{251} in domain III is the specific target for the photoinsertion into uPAR of the biradical triplet state of Bpa in AE83 (Table 5).

pH Dependence of the Receptor−Ligand Interaction. To establish the pH dependence of the uPA−uPAR interaction, 100 nM soluble uPAR was allowed to bind to immobilized uPA and complex formation was monitored in real time by surface plasmon resonance using a Biacore2000 instrument. When the recorded level of binding of uPAR is plotted as a function of pH (Figure 7), a titration curve

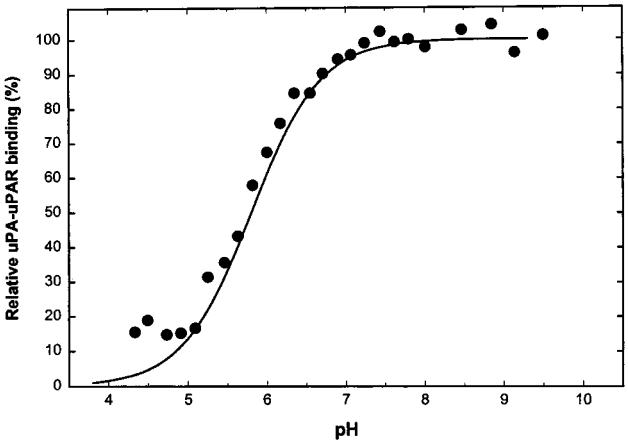

FIGURE 7: Effect of pH on the uPA−uPAR interaction. The interaction between immobilized uPA and 100 nM uPAR was monitored in real time at 5 °C by surface plasmon resonance as a function of pH using a running buffer adjusted to different pHs in the interval of 4.0−10.0. The flow path was pre-equilibrated with the relevant buffer, and the level of uPA−uPAR complex formation at that pH was subsequently measured after a fixed contact time of 7.5 min (●). Also shown is the theoretical titration curve for imidazole having a pK_a of ∼5.8 (—).

comparable to that of the imidazole side chain of a histidyl residue emerges.

DISCUSSION

Residues located at the interactive interface between uPAR and a decapeptide antagonist of uPA binding have previously been labeled by site-directed photoaffinity cross-linking using photoactivatable peptides (*12*). Receptor residues targeted by this approach are likely to coincide at least partly with the genuine uPA binding site, since the antagonist employed in several respects mimics uPA in receptor binding. First, the intact three-domain structure of uPAR is a prerequisite for a productive high-affinity interaction with either ligand (*12*, *13*, *20*). Second, the uPAR-mediated enhancement of ANS fluorescence can be titrated by addition of either ligand at a 1:1 stoichiometry, indicating that both interactions shield a surface-exposed hydrophobic patch uniquely present on the unoccupied, high-affinity conformation of uPAR (*12*, *13*). Third, the receptor binding sequences of both ligands contain

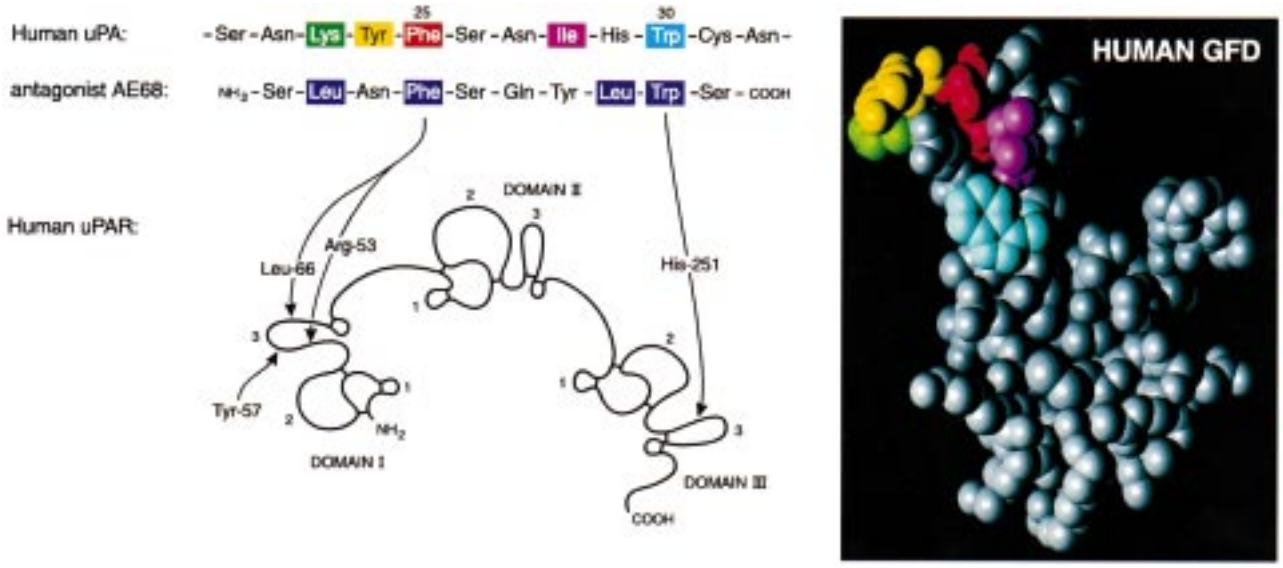

FIGURE 8: Schematic representation of residues in human uPAR targeted by site-directed photoaffinity labeling using a decamer peptide antagonist as a surrogate for uPA. To the top left is shown a linear sequence alignment of the decapeptide antagonist (AE68) with the receptor binding region (residues 21−32) in the ω-loop of the GFD of human uPA. Residues important for receptor interaction are highlighted by colored boxes in both ligands (*11*, *12*, *15*, *24*). Locations of residues in uPAR targeted by the site-specific insertion of photoprobes derived from AE68 are shown in a schematic model of human uPAR (*23*). Also shown is the position of Tyr^{57}, previously demonstrated to reside in the receptor−ligand interface (*15*). Each of the three consecutive Ly6/uPAR-type domains of the receptor is thought to adopt an overall folding topology similar to the "three-finger loop" structures of CD59 and the snake venom α-neurotoxins (see Figure 9). The locations of these putative structural loops in uPAR are designated in the model with Arabic numerals. A space filling model of the three-dimensional structure of the GFD of uPA is shown to the right as determined by NMR (*40*). Residues critical for receptor binding form a contiguous surface-exposed patch that is highlighted using a color code identical to that shown to the left for the primary sequence of uPA.

identically spaced Phe and Trp residues which are essential for their interaction with uPAR (Figure 8). Fourth, the NH_2-terminal domain I of uPAR is directly involved in the interaction with both ligands (*12*, *16*). The identification of receptor residues specifically targeted by photoaffinity labeling may therefore be expected to generate valuable information on the topology of the cognate ligand binding site for uPA.

Two different photophores attached to phenylalanine were incorporated in the photoprobes, benzophenone and (trifluoromethyl)aryldiazirine. Upon photoactivation, the former reversibly generates a rather long-lived biradical triplet intermediate capable of productive photoinsertions within a maximal range of 3.1 Å and having electron-rich C−H bonds as preferential targets for the hydrogen abstraction (*21*). In contrast, the (trifluoromethyl)aryldiazirine decomposes irreversibly upon irradiation, generating a highly reactive singlet carbene that will enforce hydrogen abstraction with no particular target selectivity, except for the requirement of spatial proximity (*22*). Combining the traditional peptide mapping protocol by enzymatic fragmentation and HPLC purification with MALDI-MS and computer searching in a database covering all theoretical tryptic peptides of uPAR greatly facilitated the present identification of the residues in uPAR targeted by the specific photoinsertions. Photoprobes replacing Phe^4 of the decapeptide antagonist AE68 selected Arg^{53} situated in uPAR domain I loop 3 as the primary target, but also to a lesser extent labeled Leu^{66} in the same loop. When Trp^9 of AE68 was replaced by *p*-benzoylphenylalanine, the primary target for the photocross-linking was His^{251} situated in loop 3 of uPAR domain III. From these studies, it is evident that the decapeptide analogues of AE68 interact with a composite ligand binding site on the receptor comprising homologous regions located within distinct structural domains of uPAR (i.e., the NH_2-terminal part of loop 3 in both domains I and III, as illustrated in Figure 8).

The involvement of loop 3 of domain I in ligand binding has previously been implicated as Tyr^{57} is protected from chemical modification by tetranitromethane in the uPAR−GFD complexes (*15*). In addition, the proximity of the ligand binding site to Asn^{52} in loop 3 of uPAR domain I is indicated by the reduced *N*-glycanase susceptibility of the carbohydrate attached to this site on binding of either pro-uPA, ATF, GFD, or the synthetic peptide antagonist (*18*).

Circumstantial evidence has previously suggested that structures outside uPAR domain I either play a modulatory role in uPA binding or are directly engaged in the interaction with uPA (*13*, *20*, *23*). The present photoaffinity labeling directly establishes the spatial proximity of His^{251} in loop 3 of uPAR domain III to the bound peptide antagonist. The selective labeling of a histidine residue in the receptor−ligand interface by the photoprobe AE83 may possibly be related to the observed pH dependence of the receptor−ligand interaction (Figure 7). The titration profile of the specific uPA−uPAR interaction measured in real time by surface plasmon resonance as a function of pH can thus be superimposed onto the theoretical titration profile of an imidazole side chain having a pK_a of ∼5.8. It should however be borne in mind that the GFD module of uPA also contains a histidine residue, although studies using site-directed mutagenesis seem to imply that His^{29} of GFD is less critical for its interaction with uPAR (*24*).

During the assignment of the photoaffinity labeling of uPAR by AE81, it was surprisingly observed that the insertion of the benzophenone moiety into Leu^{66} led to a specific chemical fragmentation of the adjacent COOH-terminal peptide bond in uPAR. No fragmentation was,

however, observed when the benzophenone moiety was replaced with (trifluoromethyl)aryldiazirine in the photoprobe AE84. This finding may provide an explanation for the unexpected difficulty encountered when sequencing past the cross-linking site of certain photoconjugates formed by an activated benzophenone moiety, a phenomenon designated "abrupt sequence termination" (*25*−*27*). Being acid-catalyzed, the proposed fragmentation mechanism may in fact be promoted by the repeated exposure to acidic conditions during the automated protein sequencing by Edman degradation.

This site-directed photoaffinity labeling study establishes the spatial proximity of uPAR domains I and III, a property necessary for the assembly of the observed composite ligand binding site. The integrity of this binding site may be expected to rely on weak interdomain interactions present only within the intact, multidomain structure of uPAR as proteolytic cleavage of the linker regions separating either uPAR domains I and II (*13*) or uPAR domains II and III (*20*) has a severe impact on the receptor affinity for uPA. Circumstantial evidence that supports this hypothesis is provided by size exclusion chromatography of chymotrypsin-treated uPAR which demonstrates a weak, noncovalent association of the liberated domain I with domains II and III (*14*). Since a three-dimensional structure has yet to be solved for uPAR or its isolated domains, a structure−function rationale for the observed photoaffinity labeling pattern can only be suggested by homology modeling. The three domains of uPAR belong to the Ly-6/uPAR domain family,[2] which includes glycolipid-anchored single-domain membrane proteins (e.g., CD59, E48, and Ly-6) as well as a large collection of secreted snake venom α-neurotoxins (*23*). Recently, another multidomain protein (Robo-1) belonging to the Ly-6/uPAR domain superfamily has been said to consist of two such domains (*28*). The putative three-dimensional consensus folding topology for the individual Ly-6/uPAR domains is represented by a "three-finger" main chain loop structure assembled on a central three-stranded, antiparallel β-sheet, as typified by the NMR structure of CD59 (*29*, *30*) and the X-ray and NMR structures determined for several snake venom α-neurotoxins (*31*). Interestingly, a subgroup of α-neurotoxins, designated κ-bungarotoxins, dimerize in solution by a strong homophilic interdomain interaction, and it has been proposed that these homodimers of κ-bungarotoxin constitute the physiologic relevant antagonist of the neuronal nicotinic acetylcholine receptor (*32*). The three-dimensional structure of κ-bungarotoxin has been solved experimentally by NMR (*33*) and X-ray crystallography (*34*), both demonstrating that dimer formation results in an extension of the central, three-stranded β-sheet of each monomer to a six-stranded β-sheet in the dimer (Figure 9). Intriguingly, many of the monomeric α-neurotoxins, whose X-ray structures have been determined, pack in the crystalline state as dimers with a similar 2-fold symmetry involving contact areas along the third loop of each participating monomer (*35*−*37*). This propensity for dimer formation by β-sheet condensation is of particular interest in relation to the composite ligand binding site in uPAR, since it positions the NH_2-terminal region of loop 3 of one monomer close to that of the other participating monomer (Figure 9). The possible interaction of uPAR domains I and III in a similar manner could thus provide the necessary scaffold for the assembly of the composite ligand binding site harboring Arg^{53} and Tyr^{57} of uPAR domain I as well as His^{251} of uPAR domain III.

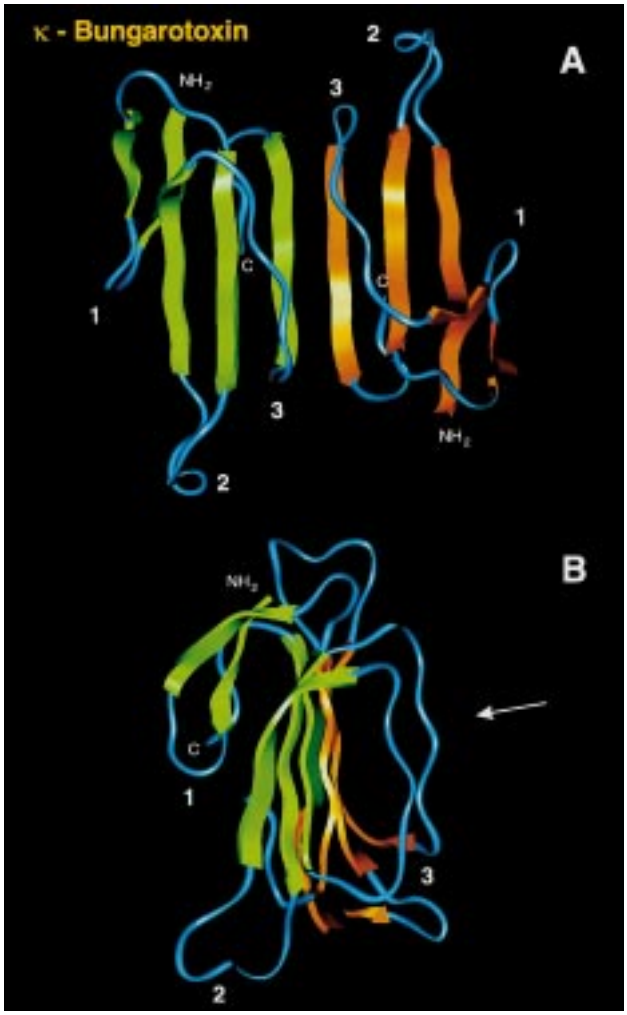

FIGURE 9: Dimeric structure of neuronal κ-bungarotoxin. These ribbon diagrams of the dimeric structure of neuronal κ-bungarotoxin were derived from the crystal coordinates deposited in the Brookhaven Protein Data Bank under code number 1KBA (*34*). A similar structure was also determined in solution by NMR (*33*, *41*). The β-sheets are represented by broad colored arrows, and the main chain loops in each monomer of κ-bungarotoxin are indicated by Arabic numerals. In panel B, the white arrow marks the NH_2-terminal region of loop 3 that is not intimately involved in the interdomain β-sheet dimerization of the κ-bungarotoxin. This region of the toxin is equivalent to areas in both uPAR domains I and III containing the residues targeted by photoaffinity labeling (i.e., Arg^{53} and His^{251}) and to the region of CD59 containing a short stretch of helical secondary structure (*29*, *30*).

Guided by the present site specific photoaffinity labeling, we are currently replacing all residues situated in loop 3 of human uPAR domains I and III by alanine using site-directed mutagenesis to determine the contribution from each individual site to the free energy of binding in the receptor interaction with either uPA or the peptide antagonist.[3] These

[3] Replacement of Arg^{53}, the primary target in uPAR domain I for the specific photoinsertion of the peptide antagonists AE81 and AE84, with either Ala or Leu by site-directed mutagenesis caused a decrease in the free energy of uPA binding ($\Delta\Delta G$) of 1.54 and 1.56 kcal/mol, respectively, for the purified uPAR mutants as derived form their binding kinetics measured in real time by surface plasmon resonance (H. Gårdsvoll, K. Danø, and M. Ploug, manuscript in preparation).

experiments may provide a useful platform for the development of new as well as refinement of existing low-molecular weight binding antagonists of the uPA−uPAR interaction with potential application for cancer therapy.

ACKNOWLEDGMENT

I thank Dr. Søren Østergaard (NOVO-Nordisk, Bagsvard, Denmark) for the synthesis of the photoactivatable peptide antagonists, Dr. Lars B. L. Hansen (Finsen Laboratory, Copenhagen, Denmark) for the synthesis of Fmoc-Tmd(Phe), and Dr. Arne L. Jensen (Department of Protein Chemistry, University of Copenhagen, Copenhagen, Denmark) for performing the amino acid composition and sequence analyses. The critical comments of Dr. Vincent Ellis (Thrombosis Research Institute, London, U.K.) are greatly appreciated as is the assistance by Dr. Bjarne Stoffer (Department of Chemistry Laboratory IV, University of Copenhagen, Copenhagen, Denmark) on the molecular graphics. The technical assistance of Helle Hymøller Hald, Helle Stærmose, and John Post is also greatly acknowledged.

REFERENCES

1. Ploug, M., Rønne, E., Behrendt, N., Jensen, A., Blasi, F., and Danø, K. (1991) *J. Biol. Chem. 266*, 1926−1936.
2. Evans, P. C., Elfman, F., Parangi, S., Conn, M., Cunha, G., and Shuman, M. A. (1997) *Cancer Res. 57*, 3594−3599.
3. Kook, Y.-H., Adamski, J., Zelent, A., and Ossowski, L. (1994) *EMBO J. 13*, 3983−3991.
4. Ossowski, L. (1988) *J. Cell Biol. 107*, 2437−2445.
5. Ossowski, L., Russo-Payne, H., and Wilson, E. L. (1991) *Cancer Res. 51*, 274−281.
6. Yu, W., Kim, J., and Ossowski, L. (1997) *J. Cell Biol. 137*, 767−770.
7. Min, H. Y., Doyle, L. V., Vitt, C. R., Zandonella, C. L., Stratton-Thomas, J. R., Shuman, M. A., and Rosenberg, S. (1996) *Cancer Res. 56*, 2428−2433.
8. Pedersen, H., Brünner, N., Francis, D., Østerlind, K., Rønne, E., Hansen, H. H., Danø, K., and Grøndahl-Nielsen, J. (1994) *Cancer Res. 54*, 4671−4675.
9. Ganesh, S., Sier, C. F., Heerding, M., Griffioen, G., Lamers, C. B., and Verspaget, H. W. (1994) *Lancet 344*, 401−402.
10. Duggan, C., Maguire, J., McDermott, E., O'Higgins, H., Fennelly, J. J., and Duffy, M. J. (1995) *Int. J. Cancer 61*, 597−600.
11. Goodson, R. J., Doyle, M. V., Kaufman, S. E., and Rosenberg, S. (1994) *Proc. Natl. Acad. Sci. U.S.A. 91*, 7129−7133.
12. Ploug, M., Østergård, S., Hansen, L. B. L., Holm, A., and Danø, K. (1998) *Biochemistry 37*, 3612−3622.
13. Ploug, M., Ellis, V., and Danø, K. (1994) *Biochemistry 33*, 8991−8997.
14. Ploug, M., Kjalke, M., Rrnne, E., Weidle, U., Høyer-Hansen, G., and Danø, K. (1993) *J. Biol. Chem. 268*, 17539−17546.
15. Ploug, M., Rahbek-Nielsen, H., Ellis, V., Roepstorff, P., and Danø, K. (1995) *Biochemistry 34*, 12524−12534.
16. Behrendt, N., Ploug, M., Patthy, L., Houen, G., Blasi, F., and Danø, K. (1991) *J. Biol. Chem. 266*, 7842−7847.
17. Barkholt, V., and Jensen, A. L. (1989) *Anal. Biochem. 177*, 318−322.
18. Ploug, M., Rahbek-Nielsen, H., Nielsen, P. F., Roepstorff, P., and Danø, K. (1998) *J. Biol. Chem. 273*, 13933−13943.
19. Weber, P. J. A., and Beck-Sickinger, A. G. (1997) *J. Pept. Res. 49*, 375−383.
20. Behrendt, N., Rønne, E., and Danø, K. (1996) *J. Biol. Chem. 271*, 22885−22894.
21. Dormán, G., and Prestwich, G. D. (1994) *Biochemistry 33*, 5661−5673.
22. Brunner, J. (1993) *Annu. Rev. Biochem. 62*, 483−514.
23. Ploug, M., and Ellis, V. (1994) *FEBS Lett. 349*, 163−168.
24. Magdolen, V., Rettenberger, P., Koppitz, M., Goretzki, L., Kessler, H., Weidle, U., König, B., Graeff, H., Schmitt, M., and Wilhelm, O (1996) *Eur. J. Biochem. 237*, 743−751.
25. Mourey, R. J., Estevez, V. A., Marecek, J. F., Barrow, R. K., Prestwich, G. D., and Snyder, S. H. (1993) *Biochemistry 32*, 1719−1726.
26. Gergel, J. R., McNamara, D. J., Dobrusin, E. M., Zhu, G., Saltiel, A. R., and Miller, W. T. (1994) *Biochemistry 33*, 14671−14678.
27. Pellicena, P., Scholten, J. D., Zimmerman, K., Creswell, M., Huang, C. C., and Miller, W. T. (1996) *Biochemistry 35*, 13494−13500.
28. Noel, L. S., Champion, B. R., Holley, C. L., Simmons, C. J., Morris, D. C., Payne, J. A., Lean, J. M., Chambers, T. J., Zaman, G., Lanyon, L. E., Suva, L. J., and Miller, L. R. (1998) *J. Biol. Chem. 273*, 3878−3883.
29. Fletcher, C. M., Harrison, R. A., Lachmann, P. J., and Neuhaus, D. (1994) *Structure 2*, 185−199.
30. Kieffer, B., Driscoll, P. C., Campbell, I. D., Willis, A. C., van der Merve, P. A., and Davis, S. J. (1994) *Biochemistry 33*, 4471−4482.
31. Dufton, M. J., and Hider, R. C. (1983) *CRC Crit. Rev. Biochem. 14*, 113−171.
32. Chiappinelli, V. A., and Lee, J. C. (1985) *J. Biol. Chem. 260*, 6182−6186.
33. Oswald, R. E., Sutcliffe, M. J., Bamburger, M., Loring, R. H., Braswell, E., and Dobson, C. M. (1991) *Biochemistry 30*, 4901−4909.
34. Dewan, J. C., Grant, G. A., and Sacchettini, J. C. (1994) *Biochemistry 33*, 13147−13154.
35. Sun, Y.-J., Wu, W.-G., Chiang, C.-M., Hsin, A.-Y., and Hsiao, C.-D. (1997) *Biochemistry 36*, 2403−2413.
36. Betzel, G., Lange, G., Pal, G. P., Wilson, K. S., Maelicke, A., and Sanger, W. (1991) *J. Biol. Chem. 266*, 21530−21536.
37. Rees, B., Bilwes, A., Samama, J. P., and Moras, D. (1990) *J. Mol. Biol. 214*, 281−297.
38. Roldan, A. L., Cubellis, M. V., Mascucci, M. T., Behrendt, N., Lund, L. R., Danø, K., Appella, E., and Blasi, F. (1990) *EMBO J. 9*, 467−474.
39. Vensel, W. H., and Tarr, G. E. (1995) in *Techniques in Protein Chemistry* (Crabb, J. W., Ed.) Vol. VI, pp 177−184, Academic Press Inc.
40. Hansen, A. P., Petros, A. M., Meadows, R. P., Nettesheim, D. G., Mazar, A. P., Olejniczak, E. T., Pederson, T. M., Henkin, J., and Fesik, S. (1994) *Biochemistry 33*, 4847−4864.
41. Sutcliffe, M. J., Dobson, C. M., and Oswald, R. E. (1992) *Biochemistry 31*, 2962−2970.

BI981203R